Proceedings of ASME Turbo Expo 2025
Turbomachinery Technical Conference and Exposition
GT2025
June 16-20, 2025, Memphis, Tennessee

GT2025-152950

NUMERICAL INVESTIGATION OF VERTICAL SPACING EFFECTS ON FLAME BEHAVIOUR AND NOX EMISSIONS IN HYDROGEN MICROMIX INJECTOR PAIRS

Guillermo González[1,*], Gaurav Singh[1], Vishal Sethi[1], David Cadrecha[2], Pedro Romero[2]

[1]Cranfield University, Cranfield, Bedfordshire MK43 0AL, UK
[2]ITP Aero, Alcobendas, Madrid, Spain

ABSTRACT

Hydrogen is emerging as a promising alternative to meet the aviation industry's ambitious CO_2 reduction targets. Its wide flammability limits enable lean combustion with low thermal NO_x emissions, but challenges such as auto-ignition and flashback risks become a significant issue due to hydrogen's high diffusivity and burning velocity. Micromix combustion addresses these challenges through a jet-in-crossflow configuration, generating miniaturised diffusion flames that enhance fuel-air mixing, reduce thermal NO_x, and mitigate flashback. Previous studies have focused on characterising air/hydrogen mixtures, improving numerical model predictions, and exploring key design parameters such as the momentum flux ratio and air gate geometry.

This study evaluates the blockage ratio (BR), a parameter that controls the vertical separation between injectors and has not been studied in isolation. Specifically, the work examines how this parameter impacts recirculation zones, flame behaviour, and NO_x emissions. Using RANS simulations with the FGM combustion model together with a thermal NO post-processing tool, variations in injector spacing were analysed while maintaining constant energy density and momentum flux ratio.

Key findings indicate that increasing injector separation reduces flame interaction, lowering thermal NO_x emissions, while excessive separation intensifies recirculation zones, increasing NO_x. The optimal blockage ratio balances these competing effects, achieving up to 15% NO_x reduction under varied conditions. These insights offer valuable design recommendations for low-emission hydrogen combustion systems.

Keywords: Hydrogen, Micromix, NOx Formation, Combustion, Injector Design

NOMENCLATURE

AGP	Air Gate Panel
BR	Blockage Ratio
CH_n	Hydrocarbon Radical
CC	Complex Chemistry
DLE	Dry Low Emissions
FGM	Flamelet Generated Manifold
GCI	Grid Convergence Index
$H_{2_{seg}}$	Hydrogen Segment
IRZ	Inner Recirculation Zone
Le	Lewis Number
LES	Large Eddy Simulation
J	Momentum Flux Ratio
NNH	Nitrogen-Nitrogen-Hydrogen
NO_x	Nitrogen Oxides
ORZ	Outer Recirculation Zone
Pr_t	Turbulent Prandtl Number
SAF	Sustainable Aviation Fuel
Sc	Schmidt Number
Sc_t	Turbulent Schmidt Number
TET	Turbine Entry Temperature
WLE	Wet Low Emissions

1. INTRODUCTION

The rise in global temperatures caused by greenhouse gases such as CO_2 has prompted regulatory authorities to take action to reduce emissions. In the field of air transport, ACARE (Advisory Council for Aviation Research and Innovation) set a target in its Flightpath 2050 to achieve a 75% reduction in CO_2 emissions and a 90% reduction in NO_x emissions by 2050, compared to 2000 baseline levels [1].

The annual growth of air traffic will make it impossible to achieve these targets using fossil fuels, requiring the implementation of alternative fuels. Sustainable Aviation Fuels (SAFs) have garnered significant interest and investment, emerging as a promising short-term solution due to their rapid applicability [2]. Electrification and hybridization, despite the inherent challenges related to battery weight, seem to be a suitable solution for short-range flights [3]. In the specific case of medium and long-range

*Corresponding author: guilleglsp5@gmail.com

Copyright © 2025 by ASME;
reuse license CC-BY 4.0

flights, hydrogen appears to be the ideal solution for achieving the goal of zero CO_2 emissions while maintaining required performance characteristics, both in range and power [4].

The implementation of hydrogen aviation requires overcoming several challenges. Firstly, there are those not directly related to the aircraft, such as the establishment of an adequate aircraft infrastructure and the development of certification regulations tailored to hydrogen [5]. Secondly, the adaptation of aircraft for hydrogen operation, due to its distinct properties compared to fossil fuels, will require significant modifications to the fuel storage and supply system, as well as a complete redesign of the combustion chambers [6].

From an overall aircraft perspective, the high energy density of hydrogen (120 MJ/kg) compared to Jet A-1 (42 MJ/kg) allows for a reduction in fuel weight, while its low density, even in the liquid state, necessitates a significant increase in the volume of the fuel tanks [7]. Fuel storage at cryogenic temperatures (20 K), coupled with hydrogen high diffusivity, complicates leak prevention and the design of heat management systems.

The combustor design, on the other hand, benefits from the properties of hydrogen. Firstly, due to its wider flammability limits compared to Jet A-1, leaner combustion is possible, thus reducing peak temperatures and NO_x emissions [8]. The high diffusivity of hydrogen, together with its high flame speed, allows for improved mixing and shorter residence times. These effects, in turn, lead to a reduction in NO_x emissions and combustion chamber length, which positively impacts the overall weight of the engines and the aircraft. Additionally, the high heat capacity could allow efficiency gains through advanced cycles that use the fuel as a heat sink. However, increase in water vapor emissions from hydrogen combustion may raise the likelihood of contrail formation [9].

Burning hydrogen in state-of-the-art lean partially premixed (LPP) combustors such as Twin Annular Premixing Swirler (TAPS) relying on a higher degree of lean-premixing could still produce higher NO_x emissions due to its high stoichiometric flame temperature compared to Jet A-1. To mitigate against the risks of auto-ignition and flashback associated with premixing while still allowing for lean-homogenous hydrogen-air mixing, a micromix (diffusion) configuration has been identified as a promising design for hydrogen injectors, as shown in Fig. 1 [8][10].

Of all the available technologies, Cranfield University has focused on developing this micromix combustion concept. The idea is to generate multiple miniaturised diffusion flames using a jet-in-cross-flow configuration, which allows the mixing length to be reduced while maximising the mixing intensity [12][13]. In addition, using a diffusion flame significantly reduces the risk of flashback, which is particularly important in hydrogen combustion. The high mixing intensity reduces the residence time required to achieve near-complete combustion, thus contributing to significantly reduced NO_x emissions. An additional positive aspect is the fuel scheduling capability, which involves selecting the fuel flow rate introduced through each of the micromix injectors across the entire cross-section of the combustion chamber. This allows for a more suitable outlet temperature distribution and better control of thermo-acoustic instabilities [14].

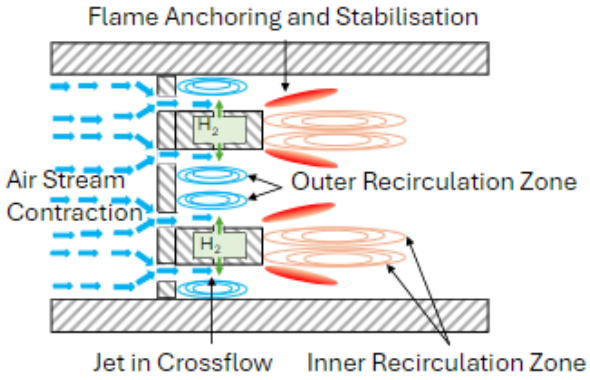


FIGURE 1: HYDROGEN MICROMIX CONCEPT [11]

As it can be seen in Fig. 1, the flow structure near the injector consists of a high-velocity air cross-flow that allows hydrogen to mix with the air. After the air guiding panel and the hydrogen segment, counter-rotating vortex pairs are formed, which anchor the flame and stabilise combustion through the recirculation of hot gases [15]. The vortex formed behind the hydrogen segment is called the Inner Recirculation Zone (IRZ), while the vortex formed after the air gate panel is known as the Outer Recirculation Zone (ORZ). In particular, the flame is stabilised in the shear layer formed between the inner and outer vortices. The reduced distance between the flame and the injection point allows a certain level of fuel mixing (partially pre-mixed flame), reducing NO_x emissions while maintaining a lower risk of flashback and auto-ignition. The recirculation regions ideally maintain a structure of isolated and miniaturized flames, which are key to reduce residence times and maximum temperatures.

This concept has been extensively tested over the last 30 years, both experimentally and numerically, by several leading universities, including Cranfield University, Aachen University, Incheon National University, and the Chinese Academy of Sciences. The concept has evolved significantly over time, with up to four generations identified, each introducing advancements in fuel-air mixing strategies leading to the current configuration [16]. In recent years, the concept has been further investigated and refined, with studies focusing on the use of different fuel mixtures and their implementation in various types of combustion chambers, whether can-type or annular.

Research in micromix combustion has been based on experiments and numerical simulations. Hydrogen flames have been characterized using a modified Borghi diagram for non-premixed flames [17], which shows that hydrogen micromixed flames lie in the transitional regime between pure flamelet and broken flames. This enables the simulation of these flames using not only LES and complex chemistry models, but also RANS models combined with the FGM combustion model, resulting in significant computational time savings.

In this paper, the impact of a design parameter related to the vertical separation between injectors on the flame structure and NO_x generation is analysed. First, the design parameters of the micromix injector are presented and their effects on the flow

Copyright © 2025 by ASME;
reuse license CC-BY 4.0

structure and emissions are assessed based on previous studies. Next, the blockage ratio (Sec. 3), the main parameter analysed in this study, is introduced, along with the explored parameter ranges and the methodology employed. The configuration of the numerical simulations is then defined, including the domain definition, boundary conditions, and model selection. Finally, the results and conclusions of the study are presented, focusing on both the overall effects on flame behaviour and the specific trends in NO_x generation.

The key contribution of this research is the differentiation of the impact of flame interactions and inner/outer recirculation zones on flow physics, flame length, flame shape, and consequently, NO_x formation. Uniquely, this analysis has been conducted for a low momentum flux ratio geometry covering values of the parameter from 0.1 to 1. To isolate the effect of flow blockage, the vertical spacing between injectors was varied by displacing the air gate while keeping the energy density, overall injector dimensions, and momentum flux ratio constant. This approach has provided new insights into novel design principles and trade-off criteria for low-NO_x hydrogen micromix injector designs, emphasizing the critical role of maintaining reduced residence times in the recirculation regions and avoiding flame merging.

2. MICROMIX INJECTOR PARAMETRISATION

The design of injectors for hydrogen micromix combustors depends on a number of geometrical parameters, which can be identified in Fig. 2. Among these parameters are: the width, height, and aspect ratio of the air gate, the diameter of the hydrogen injector, the air/H_2 offset distance, the mixing distance, and the different spacings between injectors, both vertically and horizontally [14].

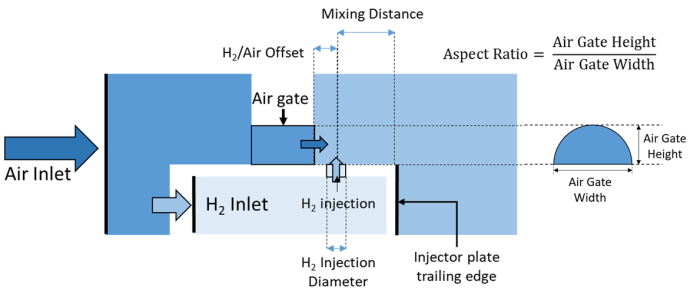


FIGURE 2: HYDROGEN MICROMIX DESIGN SPACE [11].

The different design parameters have been studied numerically and experimentally, with varying levels of detail, by institutions such as Aachen University and Cranfield University. The main objective of these studies, given the carbon-free nature of hydrogen, is to obtain a design that minimises NO_x emissions and achieves stable combustion, free of thermo-acoustic instabilities. Fuel NO_x is not a concern in the case of pure hydrogen combustion, as hydrogen does not contain fuel-bound nitrogen. The main concern, therefore, will be thermal NO formed by the Zeldovich mechanism [18], as well as NO_x produced through the NNH and N_2O pathways. In general, these NO_x formation mechanisms require high temperatures and long residence times, as they involve relatively slow reaction kinetics. Additionally, good mixing is essential to prevent regions with inhomogeneous fuel-oxidizer ratios, which could lead to the formation of hotspots and higher flame temperatures, thereby increasing NO_x emissions.

Among all the previously studied parameters, the momentum flux ratio (J) has shown a prominent importance as it defines the penetration of the fuel jet. The momentum flux ratio is defined as:

$$J = \frac{\rho_j \cdot v_j^2}{\rho_{air} \cdot v_{air}^2} \tag{1}$$

Where ρ_j is the hydrogen density, ρ_{air} is the air density, v_j is the hydrogen jet velocity, and v_{air} is the air gate velocity.

The optimum value of the momentum flux ratio is the one that ensures an adequate level of mixing while positioning the flame in the shear layer between the two vortex recirculation zones [19]. In this way, NO_x is reduced due to the reduction in flame temperatures and residence time as the flame interaction is reduced.

Low J values cause the flame to be trapped in the inner recirculation zone, leading to a significant increase in residence times at higher temperatures. The opposite occurs for high J values, as the flame is located inside the outer recirculation zone [14]. The optimum J value is characterized by maintaining adequate flame separation (Fig. 3). The main element for controlling the J is the area ratio between the air gate and the hydrogen injector.

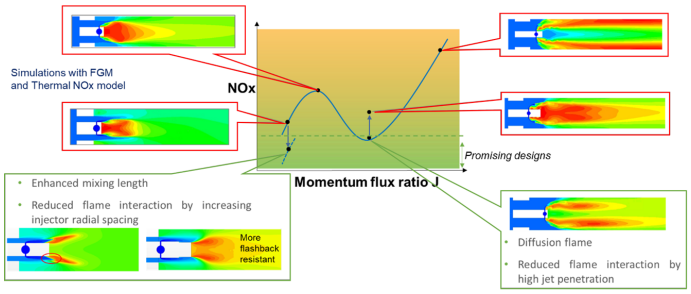


FIGURE 3: MOMENTUM FLUX RATIO EFFECT ON NO_x EMISSIONS [11]

The effects of the hydrogen penetration depth are closely related to the structure of the recirculation regions [15]. These recirculation regions are key to the stabilization and anchoring of the flame. Moreover, their structure defines both the position of the shear layer and thus the flame, as well as the residence times. The design parameters that allow the structure of these regions to be controlled will be presented in Sec. 3.

Another key parameter analyzed was the aspect ratio (height/width) of the air gates, which controls horizontal reactant mixing and the size of recirculation zones [20]. Increasing the aspect ratio reduces the outer recirculation zone but enlarges the inner zone, leading to higher NO_x generation. Perpendicular planes show that hydrogen diffusion forms a crescent shape due to counter-rotating vortices, and this diffusion improves both vertically and horizontally when lower aspect ratios are used. Similarly, studies on air gate shapes with constant area show that flatter shapes with lower aspect ratios such as as the semicircular, maintain the hydrogen diffusion in the shear layer between ORZ

Copyright © 2025 by ASME;
reuse license CC-BY 4.0

and IRZ, facilitating better mixing, and reducing NO_x emissions in the IRZ. Based on these findings, the semicircular air gate shape was selected for its optimal performance, as shown in [20].

Mixing distance has been shown to significantly impact emission levels. According to Haj Ayed et al. [21], increasing the mixing length can reduce emissions by more than 50% through improved reactant mixing. However, while achieving good overall mixing is essential for minimizing NO_x emissions, it is not the only factor to consider. The local diffusion of hydrogen, particularly the regions where the richest concentrations occur, plays a critical role in emission control [20].

Micromix systems have typically sought small injection diameters to achieve good mixing and the structure of miniaturized diffusion flames. However, these small diameters are prone to blockages and durability problems. In recent years, the trend has been to explore designs with larger injection diameters to overcome these durability issues. Studies have demonstrated that it is possible to design large-sized injectors while maintaining a well-structured arrangement of separated diffusion flames [22][23]. An additional benefit is the reduction of the sensitivity of NO_x levels to variations in operating conditions or equivalence ratios.

3. BLOCKAGE RATIO

The importance of recirculation regions has been mentioned above, as they allow flame stabilization and anchoring. In addition, by controlling their structure and dimensions, it is possible to control the position of the flame in the shear layer. Each of the recirculation regions can be controlled by two dimensionless parameters, known as blockage ratios, whose definitions are shown below [15]:

$$BR_{AGP} = \frac{h_{AGPanel}}{H_{AGPanel}} \tag{2}$$

$$BR_{H_2-seg} = \frac{h_{H_2-seg}}{H_{H_2-seg}} \tag{3}$$

The different dimensions involved in Eqs. 2-3 are represented in Fig. 4. In addition to the blockage ratios, a ratio between both of them is defined in Eq. 4 to give an idea of the relative importance of each of the recirculation regions.

$$BRDR = \frac{BR_{AGP}}{BR_{H_2-seg}} \tag{4}$$

This paper analyses the effect of these blockage ratios individually on the flow structure, flame behaviour, and NO_x generation. Unlike previous studies, in which different blockage ratios are compared, in this case, blockage ratios are modified while keeping frozen the rest of the design parameters, so that the isolated effect of the blockage ratios can be identified. To this end, parameters such as energy density, the dimensions and shapes of the injectors and air gates, the momentum flux ratio, and the mixing distance have been kept constant.

Thus, by fixing the cross-sectional area of the injector, it is possible to analyse both blockage ratios (BR_{AGP} and BR_{H_2-seg}) by modifying a single geometrical parameter. In this way BRDR captures the joint effect of both blockage ratios. All the geometry is kept constant except for the air gate, which is vertically displaced (h_{H_2-seg} is increased). The initial reference geometry corresponds to the case identified as $BR150$ in Tab. 2, and its dimensions are given in Tab. 1. These values are the result of previous studies carried out by Cranfield University as part of the EnableH2 project [24].

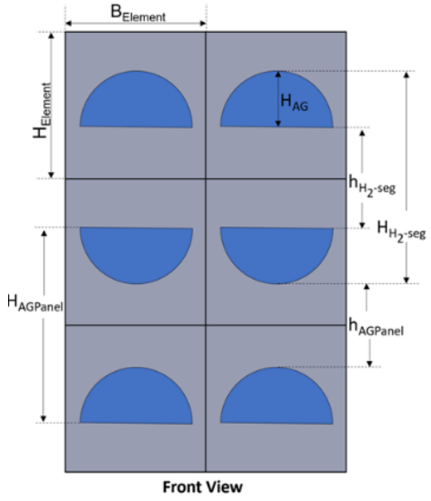


FIGURE 4: REPRESENTATIVE CROSS SECTION OF 6 MICROMIX INYECTORS

TABLE 1: DIMENSIONS OF THE REFERENCE GEOMETRY

Design Parameter	Dimension
$H_{Element}$ [mm]	3.8
$B_{Element}$ [mm]	4
H_2 Injector Diameter [mm]	0.3
B_{AG} [mm]	2.11
H_{AG} [mm]	1.055
Mixing Distance [mm]	1

Table 2 lists the different cases analysed in the exploration of the design space. Each case has been assigned an identifier to facilitate further analysis and explanation. The analysed range covers from a BRDR equal to 1, the reference case, up to a value of 0.75. The selection of the exploration ranges has sought to explore the widest possible spectrum while avoiding convergence problems. Each of the geometries has been simulated for four different equivalence ratios (ϕ), covering the range from 0.1, which corresponds to the lower flammability limit, to 0.4, above the design point conditioins.

4. METHODOLOGY

4.1 Numerical Domain and Mesh

CFD simulations has been used to carry out the investigations presented in Sec. 3. Combustion chambers based on the micromix concept require the attachment of thousands of small injectors in the form of an array. This repeatability facilitates the simulation and design of the injectors by allowing the simulation of single injectors through the exploitation of the periodicity of the flames.

Copyright © 2025 by ASME;
reuse license CC-BY 4.0

TABLE 2: DIMENSIONS AND BLOCKAGE RATIOS FOR DIFFERENT CASE IDENTIFIERS.

Case Identifier	BR100	BR110	BR120	BR130	BR140	BR150
$H_{Element}$ [mm]	4	4	4	4	4	4
$h_{H_2-seg}/2$ [mm]	1	1.1	1.2	1.3	1.4	1.5
$h_{AGPanel}$ [mm]	4	3.8	3.6	3.4	3.2	3
BR_{H_2-seg} [ ]	0.50	0.52	0.55	0.57	0.58	0.60
BR_{AGP} [ ]	0.67	0.66	0.64	0.63	0.62	0.60
$BRDR$ [ ]	0.75	0.79	0.86	0.90	0.94	1.00

The simulation domain, shown in Fig. 5, includes a pair of hydrogen injectors and their respective air gates. Periodic boundary conditions replicate the effect of adjacent injectors, while simulating a pair of injectors instead of one minimizes uncertainties these conditions may introduce on the IRZ. To reduce the influence of inlet boundary conditions on the jet-in-cross-flow region, the domain includes a 20 mm region upstream of the air gates and a partial hydrogen distribution channel upstream of the injectors. Additionally, a 100 mm channel downstream of the air gates ensures full completion and stabilization of chemical reactions.

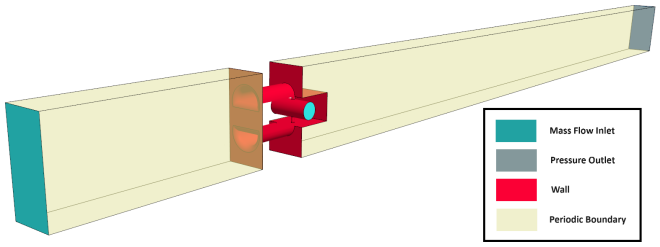


FIGURE 5: COMPUTATIONAL DOMAIN AND BOUNDARY CONDITIONS

The different boundary conditions used are represented by the colour coding in Fig. 5. The inlets of the domain have been simulated as mass flow inlets, while the outlets have been modelled as pressure outlets. As mentioned above, the side, top, and bottom faces have been selected as periodic. Finally, the injector geometry is modelled as no-slip walls.

The computational domain has been discretised using a hybrid mesh. The central region of the domain is modelled using a polyhedral mesh with a characteristic size of 0.4 mm. In the areas around the air gates and the flame zone, the mesh size is refined to 0.08 mm, and further reduced to 0.03 mm in the hydrogen injectors. This spatial discretization results in a mesh comprising approximately 1.5 million elements. This type of mesh is easier and more efficient to generate, offering lower computational costs compared to tetrahedral meshes, while achieving accuracy similar to prismatic meshes. Its selection is based on previous studies from the ENABLEH2 project, which highlighted its efficiency and cost-effectiveness [14].

The regions close to the walls make use of a prismatic mesh that reduces numerical diffusion by presenting a flow with a clearly marked preferential direction. The height of the first cell was initially selected to achieve a y^+ value of less than 1, in order to resolve the boundary layer accurately and avoid the use of wall functions. However, due to the difficulty of reaching this value at the hydrogen injection orifice, the criterion was relaxed to a y^+ value of less than 2 in this region. Additionally, a boundary layer growth factor of less than 1.5 has been used, and a smooth transition between meshes has been ensured by minimizing the cell size difference in the transition region.

The selected mesh size is the result of a mesh sensitivity analysis carried out in which both the relative error of the solution against the Richardlison Extrapolation exact value (different variables) and the available computational resources have been taken into account. The selected grid has been shown to lie in the asymptotic region of the Richardlison Extrapolation and to show Grid Convergence Index (GCI) [25] values below 0.11%.

4.2 Boundary Conditions

The boundary conditions have been obtained from results provided by the Cranfield University Performance Team. In particular, the results from the adaptation of the twin-shaft CFM LEAP 1A turbofan engine to hydrogen operation have been used. In this adaptation, the engine has been kept as similar as possible to the original engine, both in cycle parameters and size, by reducing the TET to maintain constant thrust requirements. This reduction in TET is made possible by the increased specific heat capacity of the hydrogen combustion products.

The reference pressure has been defined as the pressure at the combustion chamber inlet, which is 13.97 bar. The total inlet air temperature has been set to 748 K, equal to the combustion chamber inlet temperature. The hydrogen inlet temperature is 400 K in the reference case, based on the optimization of previous studies [14]. The turbulent variables have been estimated. The turbulent length scale has been calculated for each inlet as 7% of its hydraulic diameter, using the assumption of fully developed turbulent flow. The turbulent intensity has been approximated to a value of 5%.

The air mass flow rate per injector has been calculated preliminarily from the combustor inlet mass flow rate, taking into account cooling requirements and the dimensions of the combustion chamber. The final value obtained for each injector is 1.38 g/s. From this value, the hydrogen mass flow rate for stoichiometric combustion is adjusted by the global equivalence ratio and multiplied by the number of injectors in the domain. The exploration of the design space will be carried out for the four equivalence ratio values shown in Tab. 3.

Copyright © 2025 by ASME;
reuse license CC-BY 4.0

TABLE 3: AIR AND HYDROGEN MASS FLOW RATES

Air Mass Flow [g/s]	2.77
H_2 Mass Flow ϕ=0.1 [g/s]	4.06E-3
H_2 Mass Flow ϕ=0.2 [g/s]	8.12E-3
H_2 Mass Flow ϕ=0.3 [g/s]	1.22E-2
H_2 Mass Flow ϕ=0.4 [g/s]	1.62E-2

4.3 Models

The model selection and case configuration for the numerical analysis adhered to best practices established at Cranfield University within the ENABLEH2 project [14]. The design space exploration was conducted using RANS simulations coupled with the FGM combustion model, employing STAR-CCM+ software. The reduced computational cost of the RANS models allows for the exploration of the design space with a constrained use of resources. However, RANS simulations have drawbacks compared to LES, such as challenges in modelling turbulent-chemistry interactions and the loss of unsteady combustion behaviour [26].

The FGM combustion model offers a significant reduction in computational cost compared to the use of complex chemistry (CC) by reducing the number of transport equations to be solved. This is achieved through parametrisation of the variables and the use of pre-tabulated chemistry [27]. Flamelets are characterized by the mixture fraction Z, heat loss ratio Υ, and the progress variable c. The variability in the mixture fraction due to turbulence is represented by its variance Z_{var}. The progress variable c, indicative of the chemical status within the combustion zone, is a normalized measure computed as per Eq. 5:

$$c = \frac{y - y_u}{y_b - y_u} \tag{5}$$

Where y, y_b and y_u represent unnormalized progress variables.The unnormalised progress variable of the mixture y is defined according to Eq. 6 and y_u refers to the initial unburnt state, and y_b to the burnt state:

$$y = \sum W_i Y_i \tag{6}$$

Where y_i denotes the mass fraction of the i^{th} species and W_i its specific weight. The transport equation for unnormalised progress variable y is given in Eq. 7:

$$\omega_y = \frac{\partial \rho y}{\partial t} + \nabla \cdot (\rho u y) - \nabla \cdot (\Gamma_y \nabla y) \tag{7}$$

Where ω_y is the source term, ρ is the density and Γ_y is the diffusivity. FGM Kinetic Rate closure scheme is used to provide the source term in Eq. 7. The chemistry tables have been generated using a simplified 0D Constant Pressure reactor. The governing equations for the tabulation using the 0D Ignition reactor type are given in Eq. 8:

$$\partial T / \partial t = -\sum_{i=1}^{N} \frac{h_i (\frac{\partial Y_i}{\partial t})}{C_p} \tag{8}$$

Where C_p is the heat capacity and h_i is the enthalpy of the i^{th} species.These flamelets are the fastest and most stable to generate, but typically tend to over-predict intermediate species such as OH and CO. The turbulent-chemistry interaction is modelled using probability density functions.

The used chemical reaction mechanism developed by Naik is characterised by 9 species and 21 reactions, including intermediate species such as H, H_2O_2, HO_2, O, and OH [28]. NO and NO_x are not included in the mechanism, and their calculation method will be presented in a subsequent paragraph. The selection of this model was based on its specificity, as it was developed to simulate hydrogen combustion under the high temperature and pressure conditions typical of combustion chambers. Discrepancies between models are minimal in flame structure, concentrations, temperatures, and emissions at equivalence ratios near 0.4. However, near the flammability limit, uncertainties increase significantly, with emission differences reaching up values comparable to model error margins [29][30].

However, the main issue of the employed approach lies in the use of a chemical reaction mechanism that does not account for slow-reacting minor species like NO_x, which must be calculated using a post-processing tool [29]. This is possible due to the difference in time scales, which allows decoupling the reactions related to nitrogen oxide generation from the rest of the process. This tool solves an additional transport equation for NO, considering only the thermal NO source term, which is based on the Zeldovich mechanism. NO is considered to be a passive scalar, not influencing density calculations, and can be run as a post-processing tool for steady-state simulations or after each time step for transient simulations. The FGM combustion model, incorporating only the thermal NO pathway, underpredicts NO_x emissions, with these underpredictions potentially reaching up to 50% under peak power conditions. This discrepancy arises from the limitations of FGM in modelling the preferential diffusion of hydrogen and its exclusion of the NNH and N_2O pathways both of which are critical under high power scenarios. Nonetheless, the FGM thermal NO model's trend predictions remain valuable for design space exploration studies [29]. Since the 50% error is a consistent bias across all simulations, it predominantly influences the absolute emission values rather than the relative changes. Therefore, the relative trends, less affected by this bias, remain valid and useful for guiding explorations within the design space. For rigorous design analyses, however, it is advisable to use complex chemistry models that account for all relevant NO formation pathways. Progress variable has been defined using H_20 as the only specie to mark the combustion evolution.

The used diffusion model is based on Fick's Law and uses constant values for the dimensionless numbers Le, Sc, Pr_t, and Sc_t. These constants for the RANS-FGM model underwent calibration based on higher fidelity LES CFD [17][31] and were verified through preliminary experiments[14].The aim was to replicate the LES simulation results as closely as possible, both in terms of flame length and emission levels. The introduced values are listed in Tab. 4. This validation process, conducted against LES simulations carried out by Cranfield University, is applicable to this study as the CFD model configuration, boundary conditions, and reference geometry remain consistent. It is important to note that the use of the FGM model requires the use of $Le = 1$, which is an additional limitation of the model.

Copyright © 2025 by ASME;
reuse license CC-BY 4.0



(a) BR100 **(b) BR150**

FIGURE 6: HYDROGEN MASS FRACTION FIELD AT ϕ = 0.4

This limitation is common in commercial CFD codes. However, there are specialized codes that allow for the modification of this parameter, providing greater flexibility in modelling combustion processes.

TABLE 4: DIMENSIONLESS NUMBERS CALIBRATION AGAINST LES SIMUALTIONS

Dimensionless Number	Calibrated Value [ ]
Le	1
Sc	0.24
Pr_t	0.85
Sc_t	0.2

The selected turbulence model was the $k\omega$-SST model. This choice was made due to its improved ability to resolve flows with adverse pressure gradients. The main drawback of the model, which is its high sensitivity to boundary conditions, is mitigated by using the SST version [32]. The flow solution was obtained using the finite volume method with a segregated solver, employing the SIMPLE algorithm due to the incompressible nature of the flow, along with a second-order spatial discretization scheme and multigrid techniques to accelerate convergence.

5. RESULTS

The results of the design space exploration carried out to understand the isolated effect of blockage ratios on flow structure, flame behaviour, and NO_x emission generation are shown below. Table 2 shows the different geometries studied. It can be seen that an increase in the height of the hydrogen segment results in an increase in the blockage ratio of the hydrogen segment and a reduction in the blockage ratio of the air gate panel. The different geometries have been simulated for equivalence ratios from 0.1 to 0.4. Initially, particular features of the different cases, such as hydrogen penetration, flame structure and reaction rates, recirculation regions, or vorticity in the shear layer, are analysed. Based on this, the NO_x generation process is studied in order to properly understand it and provide design recommendations.

5.1 Hydrogen Penetration

The first aspect analysed is the penetration of hydrogen into the air jet. Previous studies have shown the existence of an optimal penetration distance [14]. Lower or higher values of this penetration distance imply the combustion of hydrogen in the recirculation regions, leading to a significant increase in residence times and thus NO_x emissions.

The main parameter available to control the penetration distance is the momentum flux ratio defined in Eq. 1. The increase of the global equivalence ratio generates an increase of J from 0.06 for ϕ = 0.1 to 0.95 for ϕ = 0.4, by increasing the hydrogen injection velocities for a constant air mass flow. Despite the increase for ϕ = 0.4, the J values obtained are still quite low, so that hydrogen dispersion will be limited to the shear layer and the IRZ, without reaching the ORZ in any case. The modification of the geometry for a constant global equivalence ratio generates minimal differences on J, thus hydrogen penetration can be considered as unchanged. The small differences observed are due to the influence of changes in the downstream pressure field in the combustion region.

On the other hand, despite the minimal influence on jet penetration, significant qualitative differences in the hydrogen distribution at the combustion region are observed in Fig. 6, especially for cases with high equivalence ratios. Higher BR cases show less diffusion of hydrogen, showing more defined boundaries. The modification of the diffusion is due to the effect of the recirculation regions, which will generate an increase of the reaction rates, causing the complete consumption of the fuel in the shear layer. Vorticity changes in the inner shear layer also play an important role, which will be discussed below.

5.2 Inner Shear Layer Vorticity

The second aspect to analyse is the vorticity in the shear layers. The vorticity values presented below have been calculated by mass flow averaging of the vorticity in a cylindrical region located in the shear layers. This vorticity, especially in the inner region, controls the mixing process between fresh gases and combustion products at the flame front, affecting flame anchoring and stability.

The vorticity in the inner shear layer shows an initial flat trend, followed by a reduction at higher blockage ratio values (Fig. 8). These vorticity variations create complex effects on the interaction with the flame structure, making them difficult to predict. High vorticity levels notably improve the mixing process, leading to faster and more efficient mixing, which increases the reaction rate. Therefore, the increase in BR and the subsequent reduction in vorticity could negatively affect the mixing process. This deterioration, in turn, may result in higher emission levels.

Copyright © 2025 by ASME;
reuse license CC-BY 4.0



(a) BR100 **(b) BR150**

FIGURE 7: OH MASS FRACTION FIELD AND STREAMLINES AT ϕ = 0.2

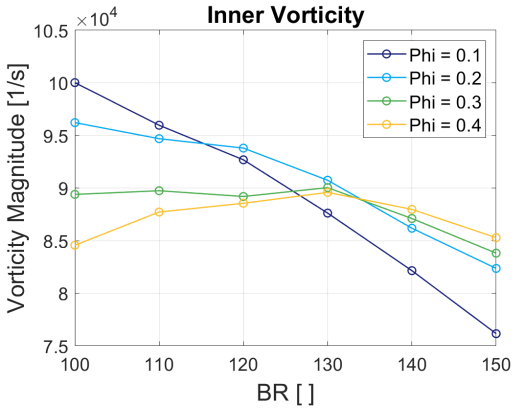


FIGURE 8: VORTICITY IN THE INNER SHEAR LAYER

This mixing deterioration effect is reflected in Fig. 6, where a lower diffusion of hydrogen in the IRZ is observed for higher BR values. This is partly due to the mixing reduction effect, but also to the intensification of combustion which causes the hydrogen under flammable conditions to be consumed faster.

5.3 Flame Structure

The third aspect to analyse is the flame structure. The flame length has been measured from the wall of the hydrogen segment to the farthest point of the 0.004 value isoline of OH mass fraction, as OH is considered a marker of the region in which hydrogen combustion is taking place. Again, it is observed for the different equivalence ratios that the effect of geometry is insignificant. Only a slight flame length reduction effect is noticeable as the BR is increased (Fig. 7) due to the increase in reaction rates. In particular, flame length is reduced a 13% from BR100 to BR150 for $\phi = 0.1$ and 10% for $\phi = 0.4$.

The most important aspect of the geometry modification on the flame behaviour is the reduction of flame interaction by increasing the flame separation (Fig. 7). To characterise this phenomenon, the mass flow rate-averaged temperature has been calculated in a cylinder with a 0.1 millimetre radius, located in the symmetry plane of the IRZ between the flames, from 5 to 10 mm downstream of the hydrogen segment wall. For $\phi = 0.1$, this temperature, which is representative of the interaction between flames, decreases from 1455 K to 1207 K between BR100 and BR150. Flame interaction leads to the formation of a region with very high flame temperatures, which generally results in a significant increase in NO_x. It is because NO_x generation is a highly localized phenomenon that scales exponentially with temperature. This effect is important not only at high equivalence ratios but also at lower values.

In addition to modifying the flame structure, the variation of the blockage ratios also has an important effect of increasing the reaction rates, as mentioned previously. To understand these effects, Fig. 9 and 10 show an axial distribution of OH mass fractions and average temperatures, obtained by mass flow rate averaging different axial cross sections.

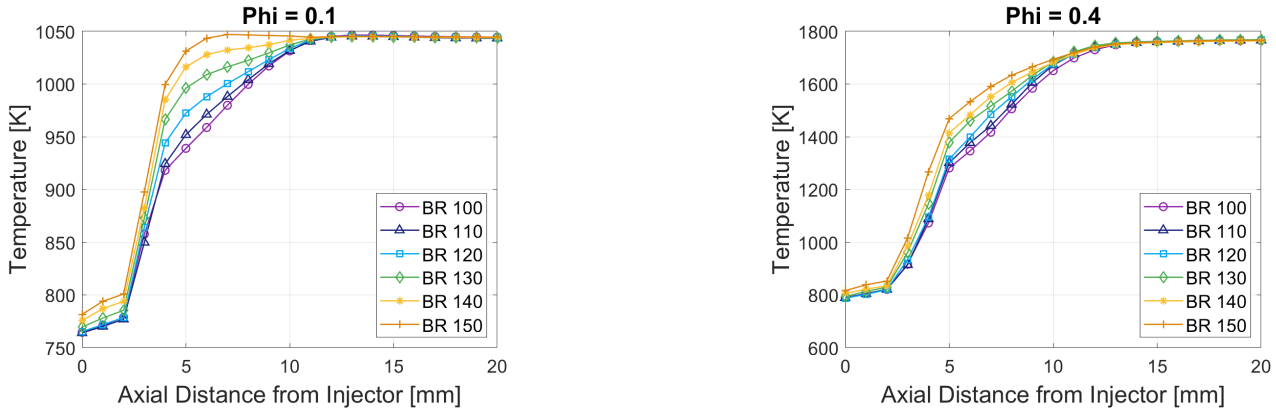
The first effect that can be observed is an increase of the average temperature in the flame region as the blockage ratio increases. This effect is explained by the intensification of combustion that is taking place, as shown by the increase in the maximum OH value and the reduction in the high OH concentration region. The intensification of combustion is not the only effect responsible for this increase in average temperatures, as there are additional effects such as the increase in the size of the recirculation region or the increase in residence time, which leads to a further increase in averaged temperatures.

A comparison of the graphs for different global equivalence ratios shows a clear reduction of the average temperature differences with increasing equivalence ratio. This is due to the increase in combustion non-stationarity, which results in the disappearance of the high OH peak that appeared for $\phi = 0.1$. In contrast, a more elongated high OH region appears with ripples in the OH mass fraction, which reduces the differences between geometries. The non-stationarity of the flames, especially for high equivalence ratios, translates into obtaining RANS solutions in which these flame oscillations are visible, as the solution does not fully converge to a steady state. Therefore, the NO_x emissions values mentioned in this paper have been obtained by time-averaging these solutions. Contours and axial distributions, however, represent instantaneous solutions, which explains variable peak positions. This non-stationary behaviour appears for equivalence ratios above 0.3.

5.4 Recirculation Regions

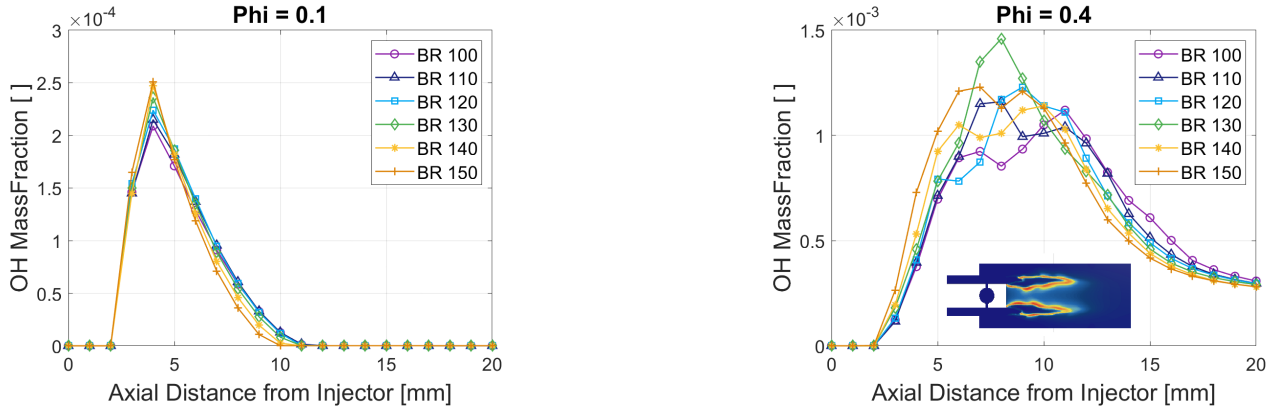
The last aspect to be analysed is the structure of the recirculation regions, in particular their size and intensity. As mentioned in Sec. 1, it is possible to identify two recirculation regions. On the one hand, the Inner Recirculation Zone, formed after the hy-

Copyright © 2025 by ASME;
reuse license CC-BY 4.0



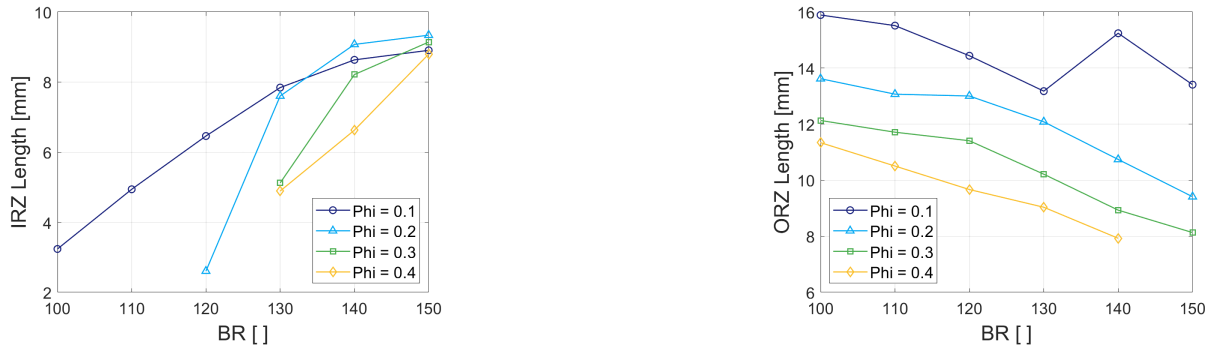
(a) ϕ = 0.1 **(b) ϕ = 0.4**

FIGURE 9: MASS-AVERAGED TEMPERATURE AXIAL DSITRIBUTION



(a) ϕ = 0.1 **(b) ϕ = 0.4**

FIGURE 10: MASS-AVERAGED OH MASS FRACTION AXIAL DISTRIBUTION



(a) IRZ **(b) ORZ**

FIGURE 11: RECIRCULATION ZONES LENGTH

Copyright © 2025 by ASME;
reuse license CC-BY 4.0

drogen segment, and the Outer Recirculation Zone, formed after the air gate panel. The length of the recirculation regions has been obtained by calculating the distance from the wall behind which they form to the farthest point of negative axial velocity.

Figure 11 shows the length variations of both regions when the geometry is modified. An increase in the length of the IRZ (+175% between BR100 and BR110 for $\phi = 0.1$) and a decrease in the length of the ORZ (-15% between BR100 and BR150 for $\phi = 0.1$) is observed as the BR increases. IRZ shows a higher sensitivity to BR than ORZ. This is due to the increase in dimensions of the hydrogen segment, after which the IRZ is formed. The ORZ shows a more linear behaviour, with a more progressive reduction in length. The IRZ, on the other hand, shows a non-linear behaviour, with a significant initial increase, followed by a region of smaller growth. This initial increase in length is due to the formation of the recirculation region itself, which is non-existent for very small hydrogen segment sizes.

This increase in size and intensity of the IRZ is of special importance in this case, as the simulations are carried out with a reduced J, which causes part of the combustion to take place inside it. In this way, NO_x generation is highly affected by these increases in IRZ size that cause significant increases in the residence times at high temperatures in the IRZ.

5.5 NOx Trends

After analysing some characteristics of the fluid field, the process of NO_x generation is further studied, since its reduction is the main objective of the design space exploration carried out. This study only considers the generation of thermal NO through the Zeldovich mechanism. The NO emissions obtained and their variations are presented in this section for the different global equivalence ratios analysed. It is important to point out that when using a RANS FGM model, it is not the values but the observed trends, which are of technical relevance.

NO Emissions values for traditional fuels are typically represented using the Emission Index ($EINO_x$), which represents the ratio between the grams emitted of a particular pollutant and the kilograms of fuel burned. This value is obtained solely by considering NO mass fraction. However, due to the difference in LHV between Jet A-1 (43.15 MJ/kg) and hydrogen (120 MJ/kg) it is common practice to make use of the Energy Based Emission Index ($EEINO_x$) to make emission values comparable between different fuels, as it is shown in Eq. 9:

$$EEINO_x = \frac{EINO_x}{LHV} \tag{9}$$

The case with equivalence ratio equal to 0.2 is the first to be analysed, as it shows the clearest trend and allows a clear explanation of the different effects observed. Figure 12 shows the variation of NO_x emissions with varying blockage ratios. From BR100 to BR110, an initial region is observed in which emissions decrease a 7% with increasing blockage ratio. The average temperature in the interaction region decreases by 9% while the velocities in the IRZ get closer to 0, but the recirculation region is not clearly formed. This shows that in spite of residence times increase, the reduction of the interaction between flames is the dominant effect. As discussed previously, as the dimensions of the hydrogen segment increase, the two flames separate, their interaction is reduced, and the temperatures in the inter-flame region are significantly reduced. This effect can be seen in the NO mass fraction fields in Fig. 12.

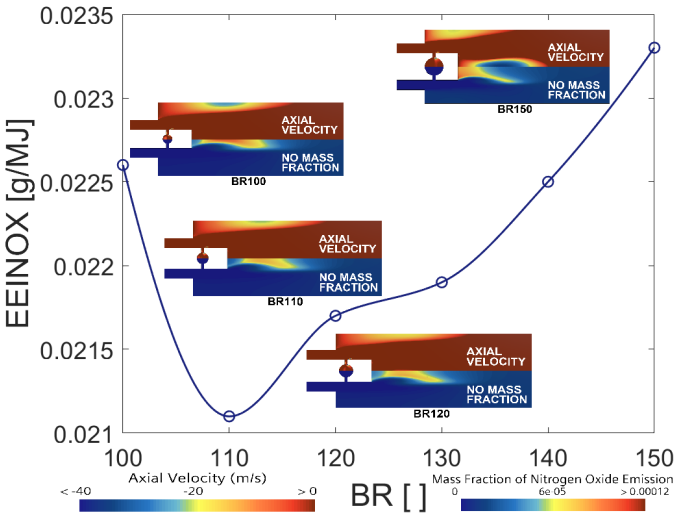


FIGURE 12: NO GENERATION AT $\phi = 0.2$

After the first decrease, the trend changes completely and NO emissions start to increase with further increases of the blockage ratio. Interaction region temperature reduces a 17% from BR110 to BR150 while IRZ gets formed (between BR110 and BR120) and its size increases a 23% from BR130 to BR150, leading to a 10% increase in NO emissions. The dominant effect in this second increase is, therefore, the rise of residence times in the high-temperature region as a consequence of the formation of the IRZ. Figure 12 shows a very similar NO formation structure between case BR110 and BR120, with NO being created in the region between flames, without showing a region of very high NO. Therefore, the increase is due to the increase in residence times as the recirculation region grows and the rise in average temperatures (Fig. 9).

Two important rises can be observed with a flatter region between them. The first one, between case BR110 and case BR120, is due to the formation of the recirculation region, as it has been explained. The second, around the BR140 case, is due to the attachment of the recirculation region, initially detached, to the hydrogen segment wall. The attachment of the recirculation region can be observed in the NO concentration, showing a reduction of NO in the inter-flame region and a significant increase near the hydrogen segment wall.

The observed $EEINO_x$ trend changes markedly with decreasing hydrogen injection, as it can be seen in the case with an equivalence ratio equal to 0.1. Figure 13 shows a clear trend of monotonically decreasing emission level with increasing blocking ratio (-26% from BR100 to BR150). This reduction in emissions is associated with a 17% decrease in the average temperature in the flame interaction region and a 175% increase in the size of the IRZ. Therefore, the emission reduction trend is again dominated by the reduction of the flame interaction. It is observed that the NO formation structure (high NO_x in the flame fronts)

Copyright © 2025 by ASME;
reuse license CC-BY 4.0

remains constant, but lower emission levels are observed due to the larger flame spacing leading to lower temperatures in the inter-flame region.

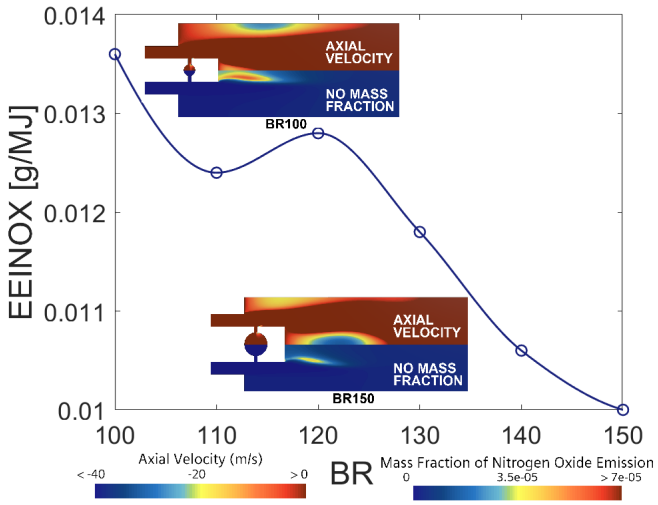


FIGURE 13: *NO* GENERATION AT $\phi = 0.1$

The slight upturn observed in the generation of *NO* around BR120 is due to the formation of a clearly defined recirculation region that increases the residence times in the high-temperature regions close to the flame. Due to the lower global equivalence ratio of the case, the temperatures in the recirculation region are not as high as in the case with equivalence ratio equal to 0.2 and, therefore, the increase in residence times does not have such a marked effect.

The case with equivalence ratio equal to 0.3 recovers the trend of the case with equivalence ratio equal to 0.2, that is, the effect of flame interaction becomes less important in favour of residence times and average temperatures. Despite a 17% reduction in the temperature between flames from BR100 to BR150, which should lead to a decrease in emissions, there is a 16% increase in emissions driven by the formation of the IRZ and a subsequent 79% increase in its size between cases BR130 and BR150. An initial slow rise between BR100 and BR120 can be observed in Fig. 14 due to the increase in mean temperatures and the intensification of the reaction in the combustion region, despite the reduction in maximum temperatures, previously to the IRZ formation.

After this first region, there is a significant increase in emissions between the BR120 and BR130 cases. This increase is due to the formation of the recirculation region, which in this case is formed directly attached to the hydrogen segment wall. The formation of this attached recirculation region generates a change in the *NO* formation structure. The *NO* levels in the inter-flame region are significantly reduced and a high *NO* region appears near the wall as it can be seen in Fig. 14. Following this substantial increase, the rate of growth of emissions slows down again between BR130 and BR150, and continues to increase because of the initial reasons, i.e. increasing average temperatures, combustion intensity and residence times.

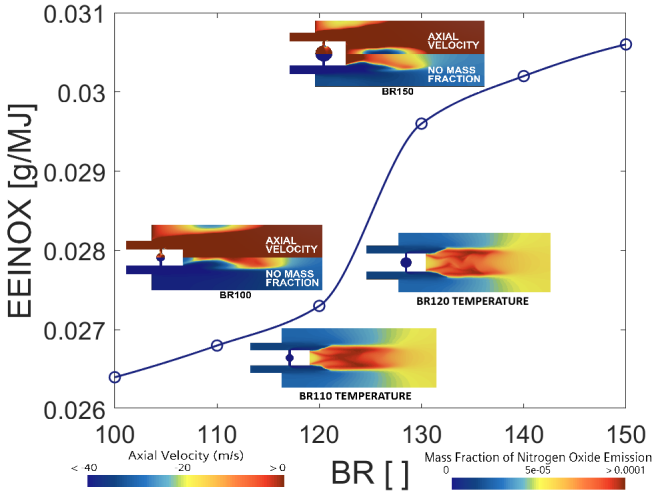


FIGURE 14: *NO* GENERATION AT $\phi = 0.3$

The case of equivalence ratio equal to 0.4 shows a trend very similar to that of the case of equivalence ratio equal to 0.2 (Fig. 15). The increasing non-stationarity of these cases, due to the increase in fuel mass flow injection, slightly reduces the importance of the recirculation regions and the interaction between flames regains importance. Thus it is possible to see from BR100 to BR110 an initial drop in *NO* emissions. The *NO* mass fraction field in BR100 shows a region of high *NO* in the flame interaction region together with a 7% reduction in the interaction region average temperature which confirms this aspect. The IRZ has not formed yet.

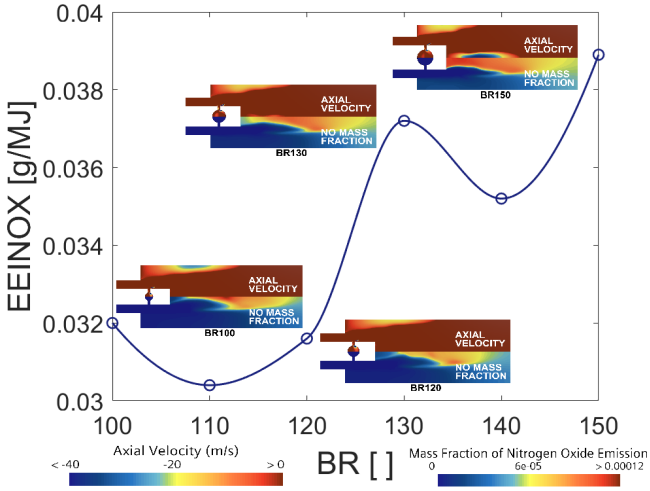
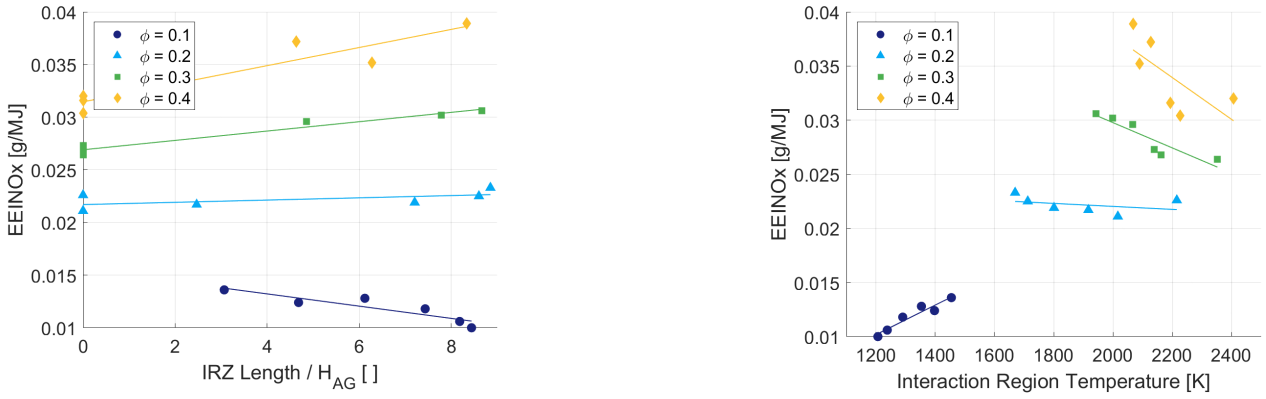


FIGURE 15: *NO* GENERATION AT $\phi = 0.4$

There is a minimum of emissions around BR110 due to the reduction of the flame interaction prior to the formation of the IRZ. There is a significant upturn generated by the formation of the recirculation region between BR120 and BR130. Figure 15 shows a very similar *NO* formation structure between BR120 and BR130 but with higher NO mass fractions, due to the effect of the increased residence times between both cases.

Copyright © 2025 by ASME;
reuse license CC-BY 4.0



(a) IRZ Length **(b) Interaction Region Temperature**

FIGURE 16: *NO* SENSITIVITY TO IRZ LENGTH AND INTERACTION REGION TEMPERATURE

Finally, after a region of moderate emission reduction due to non-stationarity of the case, a second significant increase occurs between BR140 and BR150. This is caused by the recirculation region reattaching to the wall, altering the NO generation structure and leading to a noticeable rise in NO near the wall. Between BR120 and BR150 a 23% increae in NO emissions can be observed, together with a 6% reduction in the interaction region average temperature and a 80% increase in the IRZ length. Unlike at lower global equivalence ratios, NO generation in the flame region remains significant.

To complete the decomposition of NO generation into its two main causes, Fig. 16 shows the sensitivity of NO emissions to the size of the IRZ and to the average temperature in the flame interaction region. Theoretically, both effects should lead to an increase in emissions, so positive slopes indicate that this effect is dominant, while negative slopes suggest that the effect's importance is secondary. This highlights the dominance of the flame interaction effect for $\phi = 0.1$, and the dominance of the recirculation region size, and thus residence times, for $\phi = 0.3$ and $\phi = 0.4$. For $\phi = 0.2$, the curves are flatter, indicating a balance between both effects, which is reflected in the change of trend observed in Fig. 12.

6. CONCLUSION

As a result of this research, it has been possible to know the main effects of Blockage Ratio (BR) modification on the fluid field and on NO_x generation in a hydrogen micromix injector pair. There are two main phenomena that affect NO_x generation when injector geometry is modified. Firstly, the interaction between flames is reduced with increasing BR as a consequence of the increased separation between injectors. This reduction in interaction results in a decrease in peak temperatures leading to a reduction in NO_x emissions.

Secondly, the increase in BR leads to an increase in the intensity and size of the Inner Recirculation Zone (IRZ) at the expense of the Outer Recirculation Zone (ORZ). As this is a low momentum flux ratio (J) design, part of the combustion takes place in the IRZ, resulting in increased residence times in the IRZ. This increase in residence times together with the combustion intensification and average temperature increase, as a consequence of the recirculation of hot gases, results in an increase in NO_x emissions. In addition, an important change in the NO_x formation structure has been observed when the IRZ gains intensity and attaches to the hydrogen segment wall. In this case, there is a significant increase in NO_x generation close to the wall, while NO_x in the flame region are reduced. A less important side effect is the modification of the mixing quality as a consequence of the modification of the vorticity in the shear layer.

It has been shown that the reduction of flame interaction is the dominant effect at low equivalence ratios ($\phi \approx 0.1$), leading to a reduction of the total emission level. At high equivalence ratios ($\phi \approx 0.3$), on the other hand, the increase in IRZ intensity leads to an increase in total emissions. At very high equivalence ratios, close to 0.4, the increase in flame non-stationarity again leads to a reduction of the IRZ effect in favour of flame interaction.

An optimal design should seek a balance between both effects. Too small hydrogen segments can lead to high emissions due to the formation of hot spots as a result of flame interaction, while too large hydrogen segments would lead to increases in residence times and average temperatures that would trigger emissions. This study serves as a guide to understanding the physical and chemical processes that control the generation of NO based on the modification of the blockage ratio.

Finally, it is highlighted that the modification of the blockage ratio proves to be an effective strategy for controlling emissions, allowing a reduction of up to 15% in NO_x emissions across different operating conditions compared to the reference geometry.

6.1 Limitations & Future Work

The present research has allowed to understand the effects of the Blockage Ratio (BR) on flame structure and NO_x generation for values of the momentum flux ratio (J) below 1. One of the main limitations of the model is the use of the FGM model, which is able to capture the trends in NO_x emissions. Incorporating complex chemistry together with multicomponent diffusion models [31] would allow for the consideration of all NO_x generation pathways, enabling better correlation between experimentally obtained emission levels and simulations.

Copyright © 2025 by ASME;
reuse license CC-BY 4.0

Additionally, it would be interesting to explore the design space for higher values of the momentum flux ratio (≈ 3). This would allow to reduce the influence of the IRZ in favour of the ORZ and to assess whether the trends observed in the study can be extrapolated to this case.

ACKNOWLEDGMENTS

The funding from ITP and Cranfield University for this research is gratefully acknowledged.

REFERENCES

[1] European Commission, Directorate General for Mobility and Transport, Joint Research Centre. "State of the art on alternative fuels transport systems in the European Union. 2020 update." Luxembourg: Publications Office of the European Union; 2020. https://data.europa.eu/doi/10.2771/29117.

[2] World Economic Forum. "Clean Skies for Tomorrow Sustainable Aviation Fuels as a Pathway to Net-Zero Aviation. Insight Report November 2020." Geneva (Switzerland): World Economic Forum; 2020. https://www3.weforum.org/docs/WEF_Clean_Skies_Tomorrow_SAF_Analytics_2020.pdf.

[3] Jansen, R., Bowman, C., Jankovsky, A., Dyson, R. and Felder, J. "Overview of NASA Electrified Aircraft Propulsion (EAP) Research for Large Subsonic Transports." 53rd AIAA/SAE/ASEE Joint Propulsion Conference. 2017. American Institute of Aeronautics and Astronautics. https://doi.org/10.2514/6.2017-4701.

[4] Fuel Cells and Hydrogen Joint Undertaking. "Hydrogen Powered Aviation: A Fact-based Study of Hydrogen Technology, Economics, and Climate Impact by 2050." Clean Sky2. 2020. https://op.europa.eu/en/publication-detail/-/publication/55fe3eb1-cc8a-11ea-adf7-01aa75ed71a1/language-en.

[5] Huete, J., Nalianda, D., Zaghari, B. and Pilidis, P. "A Strategy to Decarbonize Civil Aviation: A phased innovation approach to hydrogen technologies." IEEE Electrification Magazine. 2022; 10: 27-33. https://doi.org/10.1109/mele.2022.3166245.

[6] Brewer, GD. "Hydrogen Aircraft Technology." 1st Ed. New York (USA): CRC Press; 2017. https://doi.org/10.1201/9780203751480.

[7] Goodger, EM. "Hydrogen Handling in Civil Aviation: overview notes." 2nd ed. Landfall Press; 2023.

[8] Drell, IL. and Belles, FE. "Survey of Hydrogen Combustion Properties." US Goverment; 1958. NACA-TR-1383. https://ntrs.nasa.gov/citations/19930091021.

[9] Rolt, A., Nalianda, D., Rompokos, P. and Williamson, I. "Technology and scenario evaluation studies and benchmarking." European Union's Horizon 2020 research and innovation programme: EnableH2; 2023. 769241. https://cordis.europa.eu/project/id/769241/results/es.

[10] Wang, Q., McDonell, V., Steinthorsson, E., Mansour, A., Hollon, B. "Correlating Flashback Tendencies for Premixed Injection of Hydrogen and Methane Mixtures at Elevated Temperature and Pressure." ASME Turbo Expo 2009. American Society of Mechanical Engineers. GT2009-59500 https://doi.org/10.1115/gt2009-59500.

[11] Sethi, V., Sun, X., Nalianda, D. et al. "Enabling Cryogenic Hydrogen-Based CO2-Free Air Transport: Meeting the demands of zero carbon aviation." IEEE Electrification Magazine, vol. 10, no. 2, pp. 69-81, June 2022, DOI: 10.1109/MELE.2022.3165955.

[12] Suttarop, F. Daimler Chrysler Aerospace Airbus GmbH. "Method and combustor for combusting hydrogen." 2001, U.S. Pat 6,267,585 B1.

[13] Dahl, G. and Suttrop, F., "Combustion Chamber and Emissions, the Micromix Hydrogen Combustor Technology." 2001; Task Technical Report 4.4-5A, CRYOPLANE Project.

[14] Sun, X., Sethi, V., Singh, G., Giannouloudis, A., Rolt, A., Abbott, D., Gauthier, P. and Wijesinghe, C. "Final report for the single sector H2 micromix combustor segment performance and NOx emissions assessment." European Union's Horizon 2020 research and innovation programme: EnableH2; 2023. 769241. https://cordis.europa.eu/project/id/769241/results/es.

[15] Funke, H., Börner, S., Keinz, J., Hendrick, P. and Recker, E. "Low NOx Hydrogen combustion chamber for industrial gas turbine applications." 14th International Symposium on Transport Phenomena and Dynamics of Rotating Machinery, ISROMAC-14 Honolulu, Hawaii, Feb. 2012.

[16] Funke, HHW., Beckmann, N., Keinz, J. and Horikawa, A. "30 Years of Dry-Low-NOx Micromix Combustor Research for Hydrogen-Rich Fuels—An Overview of Past and Present Activities." Journal of Engineering for Gas Turbines and Power. 2021; Vol 143: Issue 7. https://doi.org/10.1115/1.4049764.

[17] López-Juárez, M., Sun, X., Sethi, B., Gauthier, P. and Abbott D. "Characterising Hydrogen Micromix Flames: Combustion Model Calibration and Evaluation." ASME Turbo Expo 2020. 2020; American Society of Mechanical Engineers. http://dx.doi.org/10.1115/GT2020-14893.

[18] Zeldovich, YB. "The oxidation of nitrogen in combustion and explosions." Acta Physicochim USSR. 1946;21:577–628.

[19] Funke, H. H.-W., Börner, S., Keinz, J., Kusterer, K., Kroniger, D., Kitajima, J., Kazari, M. and Horikawa, A. "Numerical and experimental characterization of low NOx Micromix combustion principle for industrial hydrogen gas turbine applications." ASME Turbo Expo 2012, GT2012 69421, Copenhagen, DK, June 2012.

[20] Sun, X., Agarwal, P., Carbonara, F., Abbott, D., Gauthier, P. and Sethi, B. "Numerical Investigation Into the Impact of Injector Geometrical Design Parameters on Hydrogen Micromix Combustion Characteristics." ASME Turbo Expo 2020. 2020; American Society of Mechanical Engineers. http://dx.doi.org/10.1115/gt2020-16084.

[21] Ayed, A. H., Kusterer, K., Funke, H. H.-W., Keinz, J. and Bohn, D. "CFD based exploration of the dry-low-NO x hydrogen micromix combustion technology at in-

Copyright © 2025 by ASME;
reuse license CC-BY 4.0

creased energy densities." In Propulsion and Power Research (Vol. 6, Issue 1, pp. 15–24). 2017; Elsevier BV. https://doi.org/10.1016/j.jppr.2017.01.005.

[22] Funke, HHW., Keinz, J., Kusterer, K., Haj Ayed, A., Kazari, M., Kitajima, J., et al. "Experimental and Numerical Study on Optimizing the DLN Micromix Hydrogen Combustion Principle for Industrial Gas Turbine Applications." ASME Turbo Expo 2015. June 2015; Vol. 4A: Combustion, Fuels and Emissions. American Society of Mechanical Engineers. http://dx.doi.org/10.1115/GT2015-42043.

[23] Sun, X., Morsy, M., Wijesinghe, C., Singh, G. and Sethi, V. "Numercial Investigation on the Geometrical Scaling of Hydrogen Micromix Injectors." ASME Turbo Expo 2024. 2024. American Society of Mechanical Engineers. GT2024-128859.

[24] Singh, G., Zghal, M., Sun, X., Gauthier, P. and Sethi, V. "Numerical Investigation Into the Impact of Operating Boundary Conditions on NOx Formation in Hydrogen Micromix Combustion System." ASME Turbo Expo 2023. 2023; American Society of Mechanical Engineers. https://doi.org/10.1115/gt2023-103111.

[25] Slater, JW. "Examining Spatial (Grid) Convergence." USA Goverment: NASA; 2021. https://www.grc.nasa.gov/www/wind/valid/tutorial/spatconv.html.

[26] Zghal, M., Sun, X., Gauthier, PQ. and Sethi, V. "Comparison of Tabulated and Complex Chemistry Turbulent-Chemistry Interaction Models With High Fidelity Large Eddy Simulations on Hydrogen Flames." ASME Turbo Expo 2020. 2020; American Society of Mechanical Engineers. http://dx.doi.org/10.1115/GT2020-16070.

[27] Poinsot, T. and Veynante, D. "Theoretical and numerical combustion." RT Edwards Inc; 2005.

[28] ANSYS Software. "ANSYS Chemkin Theory Manual 17.0: Reaction Design." San Diego: ANSYS, Inc; 2015.

[29] Babazzi, G., Gauthier, PQ., Agarwal, P., McClure, J. and Sethi, V. "NOx Emissions Predictions for a Hydrogen Micromix Combustion System." ASME Turbo Expo 2019. June 2019; American Society of Mechanical Engineer. http://dx.doi.org/10.1115/GT2019-90532.

[30] Agarwal, P., Sun, X., Gauthier, PQ. and Sethi, V. "Injector Design Space Exploration for an Ultra-Low NOx Hydrogen Micromix Combustion System." ASME Turbo Expo 2019: Turbomachinery Technical Conference and Exposition. 2019; American Society of Mechanical Engineers. https://doi.org/10.1115/gt2019-90833.

[31] Sun, X., Martin, H., Gauthier, P. and Sethi, B. "Sensitivity Study on Species Diffusion Models in Turbulent Combustion of Hydrogen/air Jet in Crossflow Structure." ASME Turbo Expo 2022. 2022; American Society of Mechanical Engineers. http://dx.doi.org/10.1115/GT2022-83097.

[32] Menter, FR. "Two-equation eddy-viscosity turbulence models for engineering applications[J]." AIAA journal, 1994, 32(8): 1598-1605.

Copyright © 2025 by ASME;
reuse license CC-BY 4.0

DSPACE

https://dspace.org/

Numerical investigation of vertical spacing effects on flame behaviour and NOx emissions in hydrogen micromix injector pairs

González López, Guillermo; Singh, Gaurav; Sethi, Vishal; Cadrecha Robles, David; Romero Vega, Pedro

2025-06-16
American Society of Mechanical Engineers (ASME)
https://doi.org/10.1115/gt2025-152950
González López G, Singh G, Sethi V, et al., (2025) Numerical investigation of vertical spacing effects on flame behaviour and NOx emissions in hydrogen micromix injector pairs. In: Proceeding of the ASME Turbo Expo 2025: Turbomachinery Technical Conference and Exposition, 16-20 Jun 2025, Memphis, Tennessee, USA, Volume 3A: Combustion, Fuels & Emissions, Article number GT2025-152950

Downloaded from a DSpace repository. https://dspace.org/